

A Segmentation-driven Editing Method for Bolt Defect Augmentation and Detection

Yangjie Xiao, Ke Zhang, *Member, IEEE*, Jiacun Wang, *Senior, IEEE*, Xin Sheng, Yurong Guo, Meijuan Chen, Zehua Ren, Zhaoye Zheng, Zhenbing Zhao, *Member, IEEE*,

Abstract—Bolt defect detection is critical to ensure the safety of transmission lines. However, the scarcity of defect images and imbalanced data distributions significantly limit detection performance. To address this problem, we propose a segmentation-driven bolt defect editing method (SBDE) to augment the dataset. First, a bolt attribute segmentation model (Bolt-SAM) is proposed, which enhances the segmentation of complex bolt attributes through the CLAHE-FFT Adapter (CFA) and Multipart-Aware Mask Decoder (MAMD), generating high-quality masks for subsequent editing tasks. Second, a mask optimization module (MOD) is designed and integrated with the image inpainting model (LaMa) to construct the bolt defect attribute editing model (MOD-LaMa), which converts normal bolts into defective ones through attribute editing. Finally, an editing recovery augmentation (ERA) strategy is proposed to recover and put the edited defect bolts back into the original inspection scenes and expand the defect detection dataset. We constructed multiple bolt datasets and conducted extensive experiments. Experimental results demonstrate that the bolt defect images generated by SBDE significantly outperform state-of-the-art image editing models, and effectively improve the performance of bolt defect detection, which fully verifies the effectiveness and application potential of the proposed method. The code of the project is available at <https://github.com/Jay-xyj/SBDE>.

Index Terms—Defect attribute editing, bolt defect generation, SAM, data augmentation, bolt defect detection.

I. INTRODUCTION

BOLTS are critical components for connecting and securing transmission lines, and their condition directly affects the stability and safety of the power system. Due to long-term exposure to harsh high-altitude environments, bolts are prone to defects such as missing pins or nuts caused by natural aging, environmental corrosion, and external forces. Therefore, the timely and accurate detection of bolt defects is essential to ensure the safe operation of transmission lines [1]. Traditional manual inspection methods are inefficient and

difficult to meet the needs of large-scale transmission lines. With the rapid advancement of drone intelligent inspection technologies, defect detection based on deep learning has become a primary approach in transmission line operations and maintenance [2]–[5]. However, the number of defect images in current research and practical engineering is severely limited, restricting the performance of data-driven detection algorithms. Therefore, effectively expanding defect datasets is an urgent research topic.

In recent years, some studies have focused on expanding defect datasets through generative models [6], [7]. These models fit the distribution of original data and generate defect images directly by sampling from noise. SDGAN [8] proposed a surface defect image generation method based on generative adversarial networks (GANs). It generates high-quality and diverse defect images from industrial defect-free images for expanding defect datasets. However, these methods often rely on sufficient defect images for training and may introduce unexpected random noise during generation, resulting in outputs that deviate from industrial scenarios. This direct generation method lacks precise control of defect attributes, making it challenging to meet the application requirements of object detection in complex scenarios.

It is worth noting that, although defect images are scarce, normal images are sufficient and share a high degree of feature correlation with defect images. Therefore, generating defect images through attribute editing of normal images is a more efficient and highly promising solution. However, the implementation of such methods faces challenges in capturing few-shot defect features. Currently, the conversion of normal images into defect images has become a research hotspot in the industrial field. DFMGAN [9] proposed a defect image generation method for few-sample scenarios. By training a data-efficient StyleGAN2 [10] on defect-free images and incorporating a defect-aware residual module, it achieves high-quality and diverse defect image generation. Although these methods have achieved good results, they are usually applicable to images with simple structures or uniform backgrounds. They focus on transforming one class of normal images into corresponding defect images rather than performing precise attribute editing on the same normal image [11]–[13]. Even when defects are added through generative sampling and the original image is reconstructed, the original image is inevitably changed [14]–[19].

More importantly, these existing defect conversion methods are not suited for bolt defect scenarios in the power field. The fundamental reason lies in the complexity and poor quality of bolt images, which leads to different ways of defect

Research supported by the National Natural Science Foundation of China (NSFC) under grant numbers 62076093, 61871182, 62206095, by the Fundamental Research Funds for the Central Universities under grant numbers 2022MS078, 2023JG002, 2023JC006, by the Natural Science Foundation of Hebei Province under grant number F2024502017, and by the Graduate Student Innovation Ability Training Funding Project of Hebei Provincial Department of Education under grant number CXZZBS2024167.

Y. Xiao, K. Zhang, X. Sheng, Y. Guo, M. Chen, Z. Ren, Z. Zheng and Z. Zhao are with the Department of Electronic and Communication Engineering, North China Electric Power University, Hebei, 071003, P. R. China. K. Zhang, Y. Guo and Z. Zhao are also with Hebei Key Laboratory of Power Internet of Things Technology, North China Electric Power University, Baoding 071003, Hebei, China. K. Zhang is the corresponding author (e-mail: zhangkeit@ncepu.edu.cn).

J. Wang is with the Computer Science and Software Engineering Department, Monmouth University, West Long Branch 07764, USA. (e-mail: jwang@monmouth.edu).

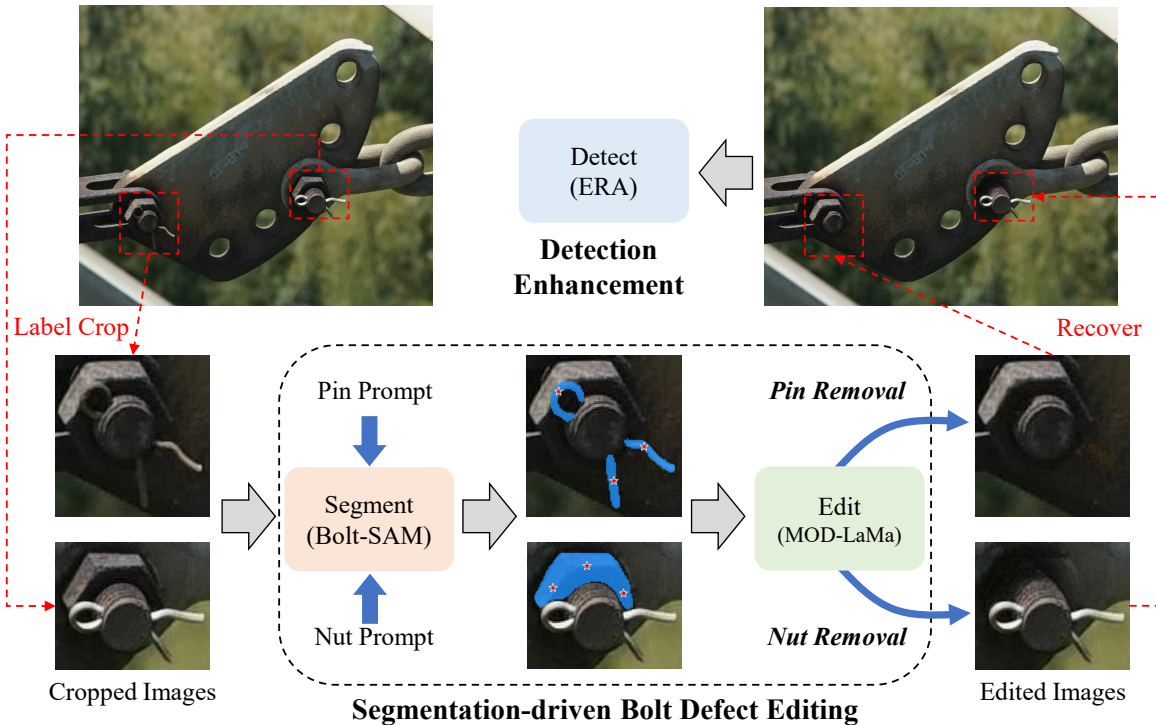


Fig. 1. The overall framework of the proposed method. SBDE combines segmentation and editing to generate defects, augmenting the defect detection dataset.

conversion. Bolts exhibit highly regular geometric shapes and defect types, necessitating editing methods that achieve high-precision attribute conversion while meeting industrial standards [6], [20]. Additionally, bolt images are typically small, with minimal pixel contrast between the bolt and its background, significantly increasing the difficulty for generative models to edit the target regions precisely. Unlike surface defects with simple backgrounds, deviations in the generation of bolt images can directly result in structural distortion, severely affecting the editing quality. Therefore, achieving accurate attribute editing for bolts requires overcoming many challenges, including precise localization of target regions, maintaining background consistency, and ensuring accurate editions of defect attributes.

To address the above issues, we propose the SBDE model that integrates Bolt-SAM for bolt attribute segmentation and MOD-LaMa for defect editing, as shown in Fig. 1. SBDE converts the images of original normal bolts into corresponding defective counterparts by accurately segmenting and editing the attributes of normal bolts. The edited defect images are used to augment detection datasets through ERA to improve the accuracy of defect detection. The contributions of this paper are summarized as follows:

- 1) We propose the first ever bolt attribute segmentation model, named Bolt-SAM. We designed CFA to enhance the extraction of bolt edge features and proposed MAMD to improve the segmentation accuracy of complex bolt attributes through multi-task fine-tuning.
- 2) We design MOD and integrate it with LaMa to construct MOD-LaMa for bolt attribute removal. By combining Bolt-SAM with MOD-LaMa, we propose the first bolt

defect attribute editing method, SBDE, which realizes the zero-defect-shot attribute editing and converts normal bolts into defect bolts.

- 3) We develop a defect detection data augmentation strategy, ERA, which seamlessly restores the edited bolt defect images into the original inspection scenes to expand the dataset. The effectiveness of our method is validated through detection experiments.

The rest of this paper is organized as follows. We first review the related work in Section II. Then, Section III describes our method in detail. After that, Section IV introduces our experiment and the experimental results. Finally, we summarize the work and discuss future work in Section V.

II. RELATED WORKS

A. Segment Anything Model

Segment Anything Model (SAM) [21] is a powerful foundational segmentation model that supports multi-modal inputs, including point prompts, box prompts, and mask prompts. It can perform zero-shot segmentation in unknown domains and demonstrates excellent performance in various vision tasks. Its generality and efficiency have rapidly made it a focal point of research in the segmentation field, inspiring numerous studies to enhance its performance in specific tasks [22], [23]. HQ-SAM [24] introduced high-quality output tokens by fusing early and final ViT features, improving the segmentation performance of SAM while maintaining its efficiency and zero-shot generalizability. SAM-Adapter [25] proposed a simple and efficient adapter mechanism that integrates domain-specific information with visual prompts, enhancing SAM's performance in complex segmentation tasks without

requiring fine-tuning of the SAM network. For low-quality image scenes, RobustSAM [26] proposed a series of anti-degradation modules to enhance the segmentation robustness of SAM under various image degradation conditions.

Additionally, some studies have further explored the impact of prompts on SAM. SAMAug [27] proposed a visual point prompt augmentation method that generates enhanced point prompts to provide SAM with more user intent information, thereby improving interactive image segmentation performance. Moreover, SAM’s powerful capabilities have been extended to other tasks. Inpaint Anything (IA) [28] proposed a new “click-and-fill” paradigm that combines SAM with various models to achieve precise localization and inpainting of target regions. Combining SAM and its related optimization methods provides robust support for addressing the challenges of attribute localization and segmentation in bolt defect editing.

B. Image Editing

Image editing has long been a key in computer vision. As a classic generative model, GAN has found extensive applications in image editing tasks [29]. StarGAN [30] and StarGAN v2 [31] proposed multi-domain translation frameworks, supporting the transformation of multiple target attributes. StyleGAN [32], StyleGAN2 [10], and StyleGAN2-ADA (ada) [33] set a benchmark in image editing by incorporating style encoding and generator architecture, allowing the generation of high-quality images with semantic disentanglement. Additionally, StyleGAN-based inversion methods, such as pSp [17], e4e [18], and ReStyle [19], achieved accurate inversion and flexible editing of real images through latent space optimization.

In recent years, the rise of diffusion models has further advanced generative technologies. DDPM [34] first introduced the diffusion process based on a Markov chain, laying the theoretical foundation for this field. Subsequently, DDIM [35] optimized generation efficiency through accelerated sampling and enabled semantic manipulation in latent space. Stable Diffusion (SD) [36], as an open-source diffusion model, has been extensively used for generation and editing tasks due to its efficient latent space operations, further driving research in diffusion models. On this basis, various fine-tuning and inversion methods have been proposed to meet the needs of different tasks [37]–[39]. DreamBooth (DB) [38] generated high-fidelity images from a small set of reference images while preserving subject features. Regarding diffusion inversion methods, Null-text Inversion [40] combined pivot inversion with text-free optimization to support flexible text-driven image editing. Negative-prompt Inversion [41] achieved efficient editing through forward propagation without requiring complex optimization, while Direct Inversion [42] employed a branching optimization strategy that significantly accelerated inference while improving editing precision.

Given the superior performance of existing generative models, numerous researchers have applied them to defect-generation tasks. SDGAN [8] generated high-quality and diverse defect samples from defect-free images to enhance

dataset diversity. Defect-GAN [11] utilized a hierarchical architecture to achieve high-fidelity generation of diverse backgrounds and random defects. DFMGAN [9] combined StyleGAN2 with a defect-aware residual module to generate diverse defect images in low-sample scenarios. StableSDG [13] adjusted the parameters of the Stable Diffusion model and the guided image generation process to produce high-fidelity steel surface defect images.

Although the above methods perform well in industrial defects, they are not suitable for bolt defect editing. Unlike general surface defects, bolt defects typically manifest as the loss of key attributes, requiring editing methods to precisely remove target regions while maintaining background consistency and preserving the original structural features. Faced with the professionalism and complexity of bolt, attribute editing based on generative models is a great challenge. In contrast, image inpainting-based approaches offer a feasible alternative. LaMa [43], a high-performing image inpainting model, enhanced inpainting quality by integrating fast Fourier convolutions and large-mask training. Further, IA [28] combined SAM with LaMa to remove the target regions. Inspired by this, we propose the SBDE. By accurately localizing and removing attributes of normal bolts, SBDE not only achieves effective bolt defect editing but also provides a novel solution for defect conversion tasks in industrial applications.

C. Bolt Defect Detection

Bolt defect detection is one of the key technologies to ensure the safe operation of transmission lines. In recent years, deep learning-based object detection methods have been widely applied in this field. AVSCNet [20] proposed an automatic visual shape clustering network to tackle the complexity of bolt shapes in transmission lines. By leveraging unsupervised clustering alongside feature enhancement, fusion, and regional feature extraction, it significantly improved the detection of missing pins. UBDDM [1] addressed ultra-small target detection by designing an ultra-small target perception module and a multi-scale feature fusion strategy. Its two-stage detection method enabled accurate bolt defect detection with minimal annotation cost. PA-DETR [44] integrated power knowledge, introduced relative position encoding and multi-scale feature extraction modules into DETR [45], and combined attribute and defect classifiers to enhance detection accuracy in visually challenging defect scenes.

Although existing methods have made progress in optimizing the structure of detection models, their exploration at the data level is still relatively limited. When bolt defect images are insufficient or data distributions are imbalanced, the performance of these methods significantly degrades. To address this issue, we propose the ERA strategy to expand the defect detection dataset, effectively improving the performance of bolt defect detection in different scenarios.

III. METHOD

To address the severe imbalance between normal and defect bolt samples in transmission lines, particularly the extreme scarcity of defect samples, we propose a segmentation-driven

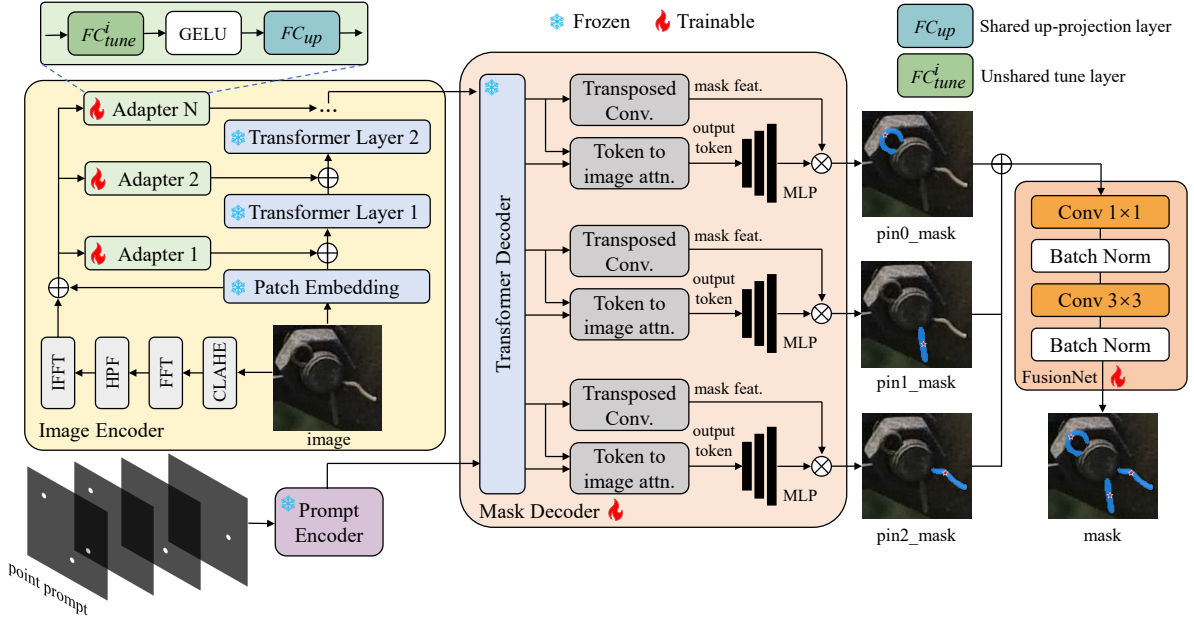


Fig. 2. The architecture of our proposed Bolt-SAM. We incorporate the adapter module into each transformer layer to enhance features and adopt a multi-task fine-tuning mask decoder architecture to improve attribute segmentation accuracy. A fusion network built with a simple MLP is employed to integrate the complete attribute mask. The parameters of the original image encoder and prompt encoder are frozen, while the adapter module, mask decoder, and fusion network are set trainable.

bolt defect editing method named SBDE. Fig. 1 shows the framework of our proposed method, where SBDE includes two core steps: segmentation and editing. It generates defect samples from normal bolt images and uses the ERA strategy to recover them into inspection images, augmenting the dataset and improving the accuracy of bolt defect detection models.

A. Segment: Bolt-SAM

In the SBDE model, the goal of the segmentation stage is to accurately extract key attribute masks from normal bolt images, providing precise segmentation regions for subsequent defect editing. To achieve this, we propose an improved segmentation model Bolt-SAM based on the baseline Robust-SAM, the structure as illustrated in Fig. 2. Taking the pin attribute of the bolt as an example, the input image first passes through the CFA module, where adaptive frequency domain information is introduced into the image encoder, resulting in enhanced image features. Then in the mask decoder, the pin is divided into three parts, and multi-task fine-tuning is performed based on corresponding point prompts to generate local masks for each part. Finally, a fusion network integrates the local masks from each part to generate a complete pin mask, thereby achieving accurate segmentation of the key attributes of the bolt.

1) *CLAHE-FFT Adapter*: The complex real-world conditions, such as lighting variations, background noise, and low-contrast regions, weaken the model’s ability to capture bolt edges, leading to inaccurate segmentation of key attributes in bolt images. To address this issue, we designed the CFA module, as shown on the left side of the image encoder in Fig. 2. CFA introduces adaptive frequency domain information into

SAM’s image encoder via simple MLPs to enhance feature representation.

Specifically, given an input image $I \in \mathbb{R}^{H \times W \times C}$, CFA first enhances details and edge features through Contrast Limited Adaptive Histogram Equalization (CLAHE) [46], resulting in an optimized image I_{cla} . I_{cla} is then transformed into the frequency domain by Fast Fourier Transform (FFT) and represented as $z = \text{FFT}(I_{cla})$. CFA constructs a high-pass filter (HPF) using a high-frequency mask M_{hpf} to extract high-frequency edge information. Following the design of the high-frequency mask in [47], M_{hpf} is defined as:

$$M_{hpf}^{i,j}(\tau) = \begin{cases} 0, & \frac{4|(i-\frac{H}{2})(j-\frac{W}{2})|}{HW} \leq \tau \\ 1, & \text{otherwise} \end{cases} \quad (1)$$

where H and W represent the height and width of the image, respectively, and τ controls the proportion of the low-frequency region. The high-frequency information is then transformed back to the spatial domain using the Inverse Fast Fourier Transform (IFFT), yielding the corresponding high-frequency component $I_{hfc} = \text{IFFT}(z \cdot M_{hpf})$:

Finally, I_{hfc} and the output of the Patch Embedding are summed to obtain the input feature F_i for the Adapter. The Adapter consists of two linear layers (FC_{tune} and FC_{up}) and an activation function GELU [48], which optimize feature representation and adjust dimensionality. The final output of the Adapter is the prompt vector P^i , defined as:

$$P^i = \text{FC}_{up}(\text{GELU}(\text{FC}_{tune}^i(F_i))) \quad (2)$$

where FC_{tune} is an adjustable linear layer unique to each adapter, used to generate prompts related to the current layer features. FC_{up} is an up-projection layer shared by all adapters,

used to adjust the prompt vector to an embedding dimension that matches the transformer input features. F_i is the sum of the linear mappings of the input. P^i is the output prompt appended to each transformer layer, serving to guide feature learning effectively.

2) *Multipart-Aware Mask Decoder*: The structural and visual complexity of bolt attributes increases the difficulty of SAM segmentation, especially as pins often appear in dispersed forms within images. To address this issue, we propose a segmented fine-tuning architecture called MAMD, illustrated on the right side of Fig. 2. MAMD employs a multi-task fine-tuning strategy, dividing the pin into three parts (pin0, pin1, pin2) for independent optimization, and generates the complete pin mask through a fusion network.

SAM’s boxes prompt is not suitable for attribute segmentation in transmission line bolt images. Due to the low resolution of bolt images and the lack of significant contrast between pixels, using boxes prompt tends to introduce excessive information from non-target regions, interfering with segmentation. In contrast, the points prompt provides more precise guidance, enabling the model to focus on the target region. It is particularly advantageous for non-contiguous structures. Therefore, we fine-tune Bolt-SAM based on points prompts. By providing points prompt for each local area of the bolt pin, we guide the model to optimize regional features to accurately capture boundary information and detail features, thereby improving the processing accuracy of non-contiguous complex structures. MAMD introduces Focal Loss and Dice Loss as loss functions. For the i -th sub-region, the local loss function is defined as:

$$L_{local,i} = \alpha \cdot L_{focal}(M_i, GT_i) + \beta \cdot L_{Dice}(M_i, GT_i) \quad (3)$$

where M_i and GT_i represent the predicted mask and ground truth mask for the i -th sub-region, respectively, while α and β are the weighting coefficients of the loss functions. MAMD integrates local mask features into a complete pin mask using a lightweight fusion network with two convolutional layers and Batch Normalization layers. The optimization of the global mask is the same as the local loss function.

MAMD effectively solves the segmentation problem of the non-contiguous structure of bolt pins through multi-task fine-tuning, providing high-quality segmentation results for subsequent bolt defect editing. Notably, for bolt nuts segmentation, we adopt only a single branch for fine-tuning.

B. Edit: MOD-LaMa

Bolt attribute editing addresses the issue of insufficient defect samples by converting normal bolts into defective ones with missing pins or nuts. Inspired by IA, we adopt an innovative image inpainting approach for editing. Leveraging its ability to integrate local features with global context, LaMa generates background-consistent content, making it particularly suitable for eliminating bolt defects. Due to the low resolution of bolt images, the masks generated by Bolt-SAM often lack sufficient contextual coverage, limiting the effectiveness of LaMa’s inpainting. We propose MOD-LaMa as shown in Fig. 3, which employs morphological operations to optimize the masks. By applying opening and dilation

operations, the method smooths boundaries and expands the target region, enhancing contextual information.

Specifically, the MOD first performs a morphological opening operation (erosion first, then dilation) on the segmentation mask, which is defined as:

$$M_{open} = (M_{seg} \ominus s) \oplus s \quad (4)$$

where M_{seg} is the initial segmentation mask, s is the structural element that controls the extent of erosion and dilation. \ominus represents the erosion operation, which is used to shrink the boundaries of the target region and remove noise from the mask. \oplus represents the dilation operation, which restores the integrity of the target region by expanding its boundaries. The definitions of erosion and dilation are as follows:

$$(M_{seg} \ominus s)(x, y) = \{o \mid (s)_o \subseteq M_{seg}\} \\ = \min_{(x,j) \in s} M_{seg}(x+i, y+j) \quad (5)$$

$$(M_{open} \oplus s)(x, y) = \{o \mid (s)_o \cap M_{open} \neq \emptyset\} \\ = \min_{(x,j) \in s} M_{open}(x+i, y+j) \quad (6)$$

where (x, y) is the coordinates of the origin of the current structural element, while (i, j) denotes the offset relative to the origin. s_o is the spatial translation of the structural element within the mask. Then, the MOD further performs a dilation operation on M_{open} , generating the final optimized mask.

$$M_{MOD} = M_{open} \oplus s \quad (7)$$

Finally, LaMa uses the MOD-optimized mask M_{MOD} together with the original image I_{ori} to repair the target region, effectively achieving bolt defect attribute editing.

$$I_{edit} = \text{LaMa}(I_{ori}, M_{MOD}) \quad (8)$$

C. Detect: ERA

To further validate the effectiveness of SBDE, we propose the ERA strategy. ERA is based on inspection images and expands the bolt defect detection dataset by generating defect samples through editing and recovering them to the original inspection scenes. The overall process is shown in Fig. 4. Specifically, we use LabelImg to annotate normal bolts in inspection images I_{ins} , crop them to extract individual normal bolt I_{ori} , and edit them with SBDE to generate defect bolt I_{edit} . Finally, I_{edit} is restored to its original position in I_{ins} with the label updated to defect, forming defect-augmented inspection images I_{aug} . The recovery operation as follows:

$$I_{aug}(i, j) = \begin{cases} I_{edit}(x', y'), & \text{if } (x, y) \cap R_{box} \\ I_{ins}(x, y), & \text{otherwise} \end{cases} \quad (9)$$

where R_{box} is the bounding box, and (x', y') refers to the corresponding coordinate mapping in I_{edit} .

The ERA-augmented inspection image fully retains the original transmission line scene information, generating defects only in localized bolt regions. This allows the detection model to learn diverse defect features within the same background, enriching the data distribution for defect detection and thereby improving detection performance. Furthermore, ERA avoids over-reliance on real defect data during data augmentation, providing an effective solution for bolt defect detection in scenarios with few-shot (or even zero-shot) defect samples.

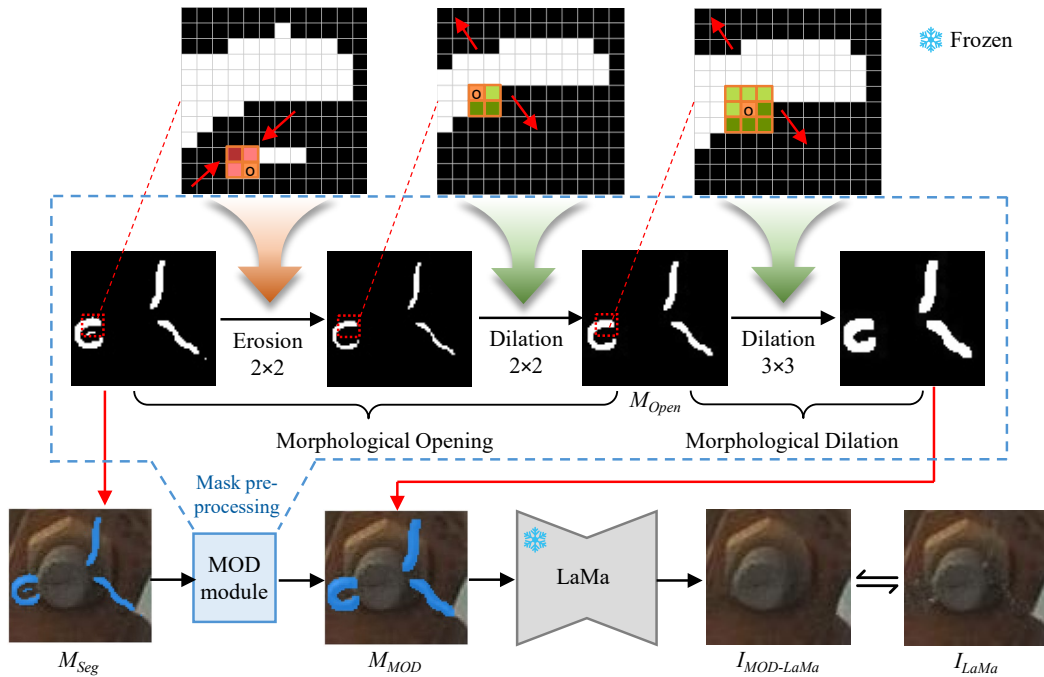


Fig. 3. Structure of MOD-LaMa. The interaction rules of the structural element s : light areas show intersections with the mask, while dark areas indicate no overlap. For erosion, o is retained only if all pixels of s fit within the mask (any deep red sets o to 0). For dilation, o is retained if any part of s overlaps with the mask (any deep green sets o to 1).

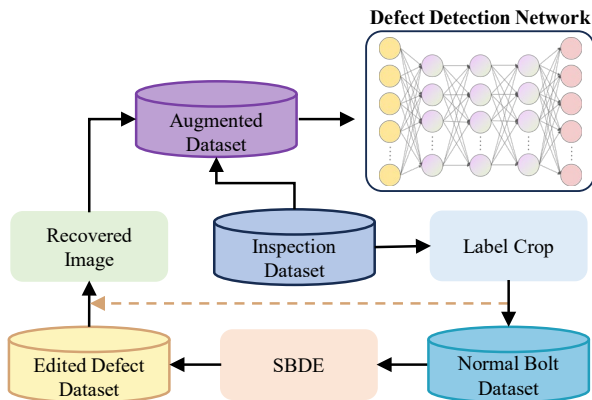


Fig. 4. The workflow of ERA, which includes inspection image cropping, bolt editing, and defect recovery. It augments the inspection dataset for defect detection networks.

IV. EXPERIMENTS

A. Datasets

We constructed the Bolt Defect Detection dataset (BDD) by collecting aerial images of transmission lines through drone inspection and annotating the bolts in the images using the LabelImg tool. BDD includes three bolt states: normal, pin losing, and nut losing, which are used for scene-level defect detection. On this basis, the inspection images are cropped according to the annotation information to extract individual bolt images, which are further filtered to construct the Bolt Defect Generation dataset (BDG). BDG supports the training of other defect generation methods for comparison with our method. SBDE focuses on the segmentation and editing of

TABLE I
DATA DISTRIBUTION OF THE BDD DATASETS.

Class	Train	Test	Total
Inspection images	1433	337	1770
Number of instances			
Normal	3961	1018	4979
Pin losing	449	100	549
Nut losing	244	63	307
All	4654	1181	5835

TABLE II
DATA DISTRIBUTION OF THE BDG DATASETS.

Class	Number of bolt images
Normal	1393
Pin losing	517
Nut losing	300
All	2253

normal bolts, utilizing only normal bolt images from BDG and excluding any defect samples. To this end, we screened normal bolt images from BDG and annotated their pin and nut attributes with masks using the Labelme tool to construct the Bolt Attribute Segmentation dataset (BAS). In BAS, the pin attribute was finely divided into three parts: the head (pin0), the left pin (pin1), and the right pin (pin2). The three datasets target different tasks and application scenarios, with examples shown in Fig. 5 and specific data distribution detailed in Table I, Table II, and Table III.

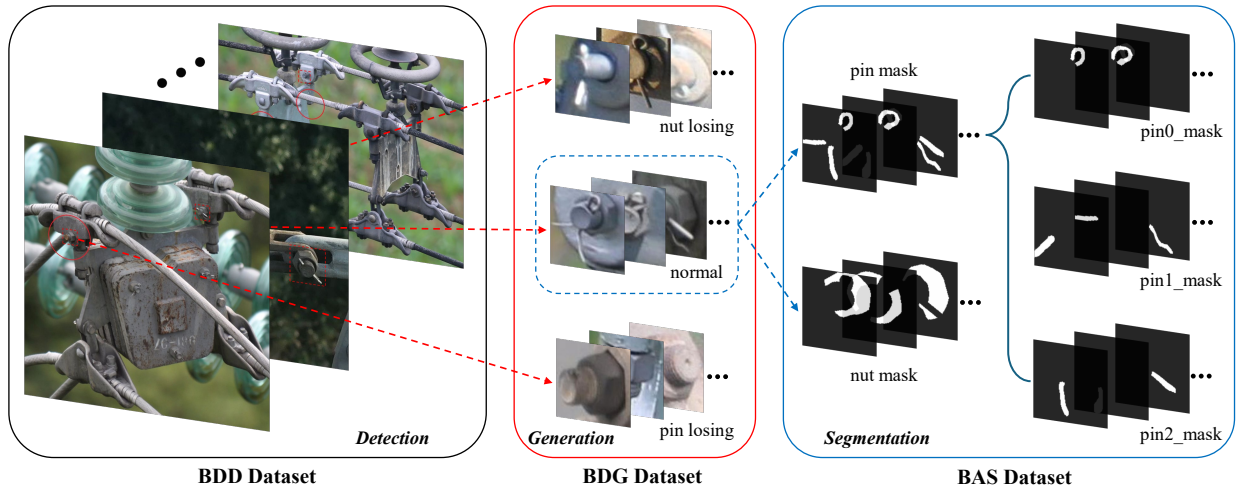


Fig. 5. The construction process of the three datasets. They are obtained by annotating, cropping, and filtering the transmission line inspection images, where BAS only contains normal bolts and the pin attributes are divided into multiple masks.

TABLE III
DATA DISTRIBUTION OF THE BAS DATASETS.

Attribute masks of normal bolts	Train	Test
Nut_mask	886	220
Pin_mask	886	220
Pin0_mask	886	220
Pin1_mask	886	220
Pin2_mask	886	220

B. Implementation Details

During the training, Bolt-SAM fine-tunes only the parameters of CFA and MAMD while freezing the rest of the parameters. Bolt-SAM adopts the points as prompts, randomly sampling three points from the ground truth mask for training. The training configuration includes a learning rate of 0.0001, a batch size of 2, and a total of 50 epochs. The experiments are conducted on two NVIDIA 4090 GPUs, implemented using PyTorch 2.4, CUDA 12.1, and Python 3.10. In MOD-LaMa, the opening operation uses an asymmetric 2×2 structural element, while the dilation operation employs a centrally symmetric 3×3 structural element. MOD-LaMa performs direct inference based on the pre-trained LaMa without additional fine-tuning. In ERA, the state-of-the-art YOLOv11 [49] detection algorithm is employed to evaluate the effectiveness of SBDE.

C. Evaluation metrics

To comprehensively evaluate the performance of SBDE, we selected different evaluation metrics for various tasks. For the segmentation, the mean Intersection over Union (mIoU), Dice coefficient (Dice), and Pixel Accuracy (PA) are used to assess the quality of the bolt attribute masks. For the detection, the mean Average Precision (mAP), Precision (P), and Recall (R) are employed to validate the bolt defect detection performance of ERA.

Due to the significant differences between SBDE and traditional generative models in editing, different evaluation metrics are employed in comparative and ablation experiments. For the comparative experiments, we focus on evaluating the quality of the edited images and their overall similarity to the original images. Peak Signal-to-Noise Ratio (PSNR), Structural Similarity Index Measure (SSIM), and Learned Perceptual Image Patch Similarity (LPIPS) are used to measure the differences between the edited images and the original images.

However, in the ablation experiments, SBDE edits only the mask region, making traditional metrics insufficient for evaluating the actual effect of bolt editing. To address this, we introduce two metrics focused on attribute editing performance: Attribute Editing Accuracy (AEA) and Human Preference Score (HPS). Among them, AEA uses a pre-trained bolt defect classification model to evaluate whether the edited bolt image can be correctly classified as the target defect type, thereby measuring the accuracy of defect conversion. The definition is as follows:

$$AEA = \frac{\sum_{i=1}^N \mathbb{I}(f_{cls}(I_{edit}^i) = y_{target})}{N} \quad (10)$$

where N represents the total number of edited images, I_{edit} denotes the edited image, y_{target} indicates the target defect category, $f_{cls}(\cdot)$ refers to the pre-trained bolt defect classification model, and $\mathbb{I}(\cdot)$ is an indicator function that equals 1 if the editing is correct and 0 otherwise. HPS is a metric more aligned with human visual judgment. The specific rules are as follows: for defect images edited by M sets of ablation experiment configurations, an expert group ranks them and assigns scores $S_{i,k} = \{1, 2, \dots, M\}$, where each score is unique. A higher score indicates better editing performance. HPS is defined as:

$$HPS = \frac{\sum_{i=1}^N \sum_{k=1}^K S_{i,k}}{N \cdot K} \quad (11)$$

where $S_{i,k}$ represents the score given by expert i to the k -th image, N denotes the number of experts, K represents the

TABLE IV
RESULTS OF ABLATION STUDY ON BOLT-SAM SEGMENTATION. THE BEST RESULTS ARE MARKED IN BOLD.

Method	CFA	MAMD	Pin			Nut		
			mIoU(%) ↑	Dice(%) ↑	PA(%) ↑	mIoU(%) ↑	Dice(%) ↑	PA(%) ↑
B1			71.16	82.80	97.48	70.44	81.90	92.76
B2	✓		74.83	85.43	97.86	76.78	86.47	94.71
B3		✓	73.75	84.72	97.90	-	-	-
B4	✓	✓	75.66	86.01	98.02	-	-	-

total number of edited images, and M refers to the number of ablation experiment configurations.

D. Ablation study

To verify the specific contributions of each module in our method, we conducted two ablation studies, evaluating the segmentation performance of Bolt-SAM and the editing effectiveness of SBDE. All experiments were performed on the BAS dataset.

1) *Ablation Study on Bolt-SAM Segmentation:* Bolt-SAM is the core algorithm of SBDE, focusing on generating high-quality bolt attribute masks. To validate the effectiveness of the CFA module and the MAMD architecture, we conducted segmentation ablation experiments, with quantitative results presented in Table IV. Compared with the baseline model (B1), the proposed modules showed significant improvements across all metrics. The CFA module (B2) demonstrated particularly notable enhancements in nut attributes, with mIoU, Dice, and PA increasing by 6.34, 4.57, and 1.95, respectively. This is because nuts are located at the bottom of bolts and are prone to shadowing effects caused by lighting, leading to blurred and indistinguishable edges, while effectively mitigated by CFA. MAMD (B3) is a multi-stage architecture designed for pins, which achieved more precise localization of pin components and outperformed B2 in terms of the PA metric. It is important to note that PA measures the overall pixel accuracy, and due to the small size of bolt images, the improvement in PA is relatively limited, especially for pin attributes. Overall, Bolt-SAM (B4) combines CFA and MAMD, balances the unique characteristics of bolt attributes, and achieves the best results across all metrics. Fig. 6 shows the visualization results of the improved module on pin segmentation, among which B4 achieves the best segmentation effect.

2) *Ablation Study on SBDE Editing:* SBDE achieves precise editing of bolt defect attributes by combining Bolt-SAM and MOD-LaMa. To validate the contributions of these two core modules, we designed ablation experiments for the editing task, using AEA and HPS as evaluation metrics, as described in Section 4.3. The experiments included four ablation configurations, with each configuration generating 300 edited images. The scores were provided by 20 domain experts. Quantitative results are presented in Table V, and Fig. 7 shows a visual comparison of editing results across different module configurations.

The Baseline (S1) uses a combination of RobustSAM and LaMa, and the editing effect performs the worst, with both AEA and HPS at the lowest levels. After introducing Bolt-SAM (S2), segmentation accuracy slightly improves, but the

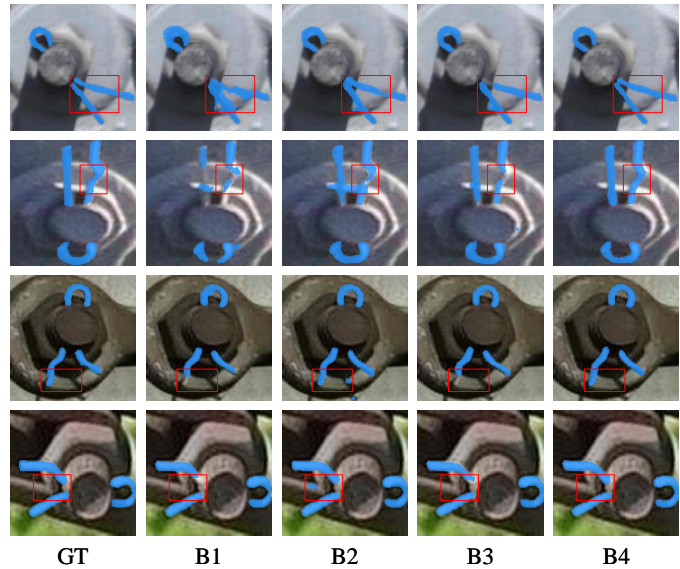


Fig. 6. Visualization of Ablation Results for Bolt-SAM Segmentation Based on Pin Attributes

TABLE V
RESULTS OF ABLATION STUDY ON SBDE EDITING. THE BEST RESULTS ARE MARKED IN BOLD.

Method	Bolt-SAM	MOD-LaMa	Pin		Nut	
			AEA(%) ↑	HPS ↑	AEA(%) ↑	HPS ↑
S1			11.83	1.17	9.92	1.08
S2	✓		13.17	1.83	11.78	2.14
S3		✓	78.63	3.2	69.82	2.87
S4	✓	✓	85.89	3.8	77.17	3.91

overall editing effect remains poor, particularly in correctly editing attributes (as shown in Fig. 7 for S1 and S2). In contrast, with the addition of MOD-LaMa (S3), editing performance improves significantly, demonstrating that morphological optimization plays a critical role in refining mask regions and enhancing editing quality. The substantial improvement in AEA indicates that attributes were effectively edited (as shown in Fig. 7 for S3). SBDE (S4) combines the advantages of Bolt-SAM and MOD-LaMa, which achieves the best performance across all metrics. Specifically, AEA for pins and nuts reaches 85.89 and 77.17, respectively, while HPS scores reach the highest values of 3.8 and 3.91, indicating superior editing results (as shown in Fig. 7 for S4).

In summary, Bolt-SAM enhances segmentation quality, and MOD-LaMa optimizes the editing region. Their synergistic

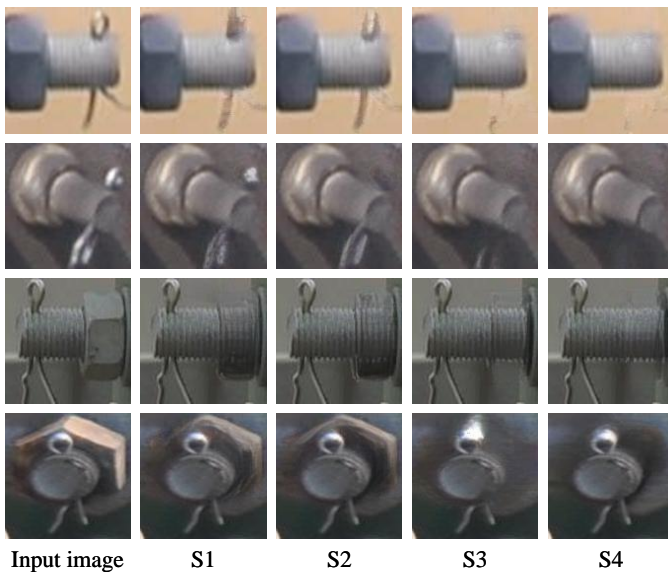


Fig. 7. Visualization of Ablation Results for SBDE Editing

integration significantly improves SBDE’s performance in bolt defect attribute editing.

E. Comparison with existing methods

To comprehensively validate the performance advantages of the SBDE in segmentation and editing, we conducted detailed comparisons with state-of-the-art segmentation and editing methods. The comparative experiments are divided into two parts: segmentation performance comparison for Bolt-SAM and editing effectiveness comparison for SBDE.

1) *Comparative experiment of Bolt-SAM Segmentation:* In the segmentation, we compared Bolt-SAM with SAM, SAM-Adapter, HQ-SAM, and RobustSAM, while also exploring the impact of the number of point prompts on bolt attribute segmentation performance. It is important to note that point prompts refer to the number of positive prompt points set for each part of the pin. The experiments are conducted on the BAS dataset, with all comparison methods fine-tuned. Segmentation performance is evaluated using three metrics: mIoU, Dice, and PA.

The quantitative results, as shown in Table VI, indicate that Bolt-SAM significantly outperforms all other methods across all metrics, achieving the best performance when using the 3-points prompt (which is adopted as the default setting in all other experiments in this paper). Compared with the baseline, Bolt-SAM improves the mIoU, Dice, and PA in pin segmentation by 4.50, 3.21, and 0.54, respectively, and improves the nut segmentation by 6.34, 4.57, and 1.95.

Further analysis of the impact of the number of point prompts on model performance shows that increasing the number of prompts generally improves segmentation results. This effect is particularly evident in Bolt-SAM’s pin segmentation, where using the 3-points prompt improve mIoU, Dice, and PA by 2.93, 3.13, and 0.41, respectively, compared to a 1-point prompt. This is because the pixels of the bolt pins are too small, and more prompts can help the model better capture the

boundaries of the target region. This is the opposite in SAM’s pin segmentation, reflecting SAM’s strong generalization.

Fig. 8 shows the segmentation results of different methods. It can be observed that the masks generated by Bolt-SAM have clearer boundaries and are highly consistent with the ground truth masks. Even under complex background interference, Bolt-SAM accurately captures the edge information of bolt attributes, while other methods exhibit obvious boundary blurring and missed and false detection of target regions.

2) *Comparative experiment of SBDE Editing:* The editing principle of SBDE is different from the mainstream editing methods. Since no similar methods currently exist, we compare SBDE with state-of-the-art GAN-based and diffusion-based editing methods, including StarGANv2, ReStyle+e4e, Null-text Inversion, Negative-prompt Inversion, and Direct Inversion. All comparison methods are trained or fine-tuned on the BDG dataset, with PSNR, SSIM, and LPIPS used as evaluation metrics. It is important to note that SBDE does not rely on any defect images. Instead, it is a zero-defect-shot editing method based on the pre-trained LaMa, directly generating defect images from normal ones.

The quantitative results in Table VII demonstrate that SBDE significantly outperforms the comparison methods in all metrics. Compared to the best-performing methods, SBDE improves PSNR and SSIM for pin defect editing by 7.48 and 5.82, respectively, while reducing LPIPS by 26.98. For nut defect editing, SBDE improves PSNR and SSIM by 4.38 and 2.88, respectively, while reducing LPIPS by 21.67. This advantage stems from SBDE’s precise editing within the target region while preserving the rest of the image intact, thus outperforming the generation method in both pixel level and perceptual quality.

Fig. 9 shows a visual comparison of editing results across different methods. SBDE generates defect images that are highly consistent with the realistic perception of defects, with the natural target region editing and intact backgrounds. In contrast, StarGANv2 and ReStyle+e4e tend to search for latent vectors in the generative space that semantically align with the corresponding defect, resulting in significant deviations from the original image and poor convergence. Although Null-text Inversion, Negative-prompt Inversion, and Direct Inversion maintain high fidelity across the entire image, their editing in the defect region is suboptimal, often introducing unnecessary artifacts or distracting information. This is due to domain gaps encountered during the fine-tuning of Stable Diffusion and limitations arising from differences in training data, which hinder the editing effectiveness of large model-based methods.

F. Bolt defect detection with ERA

To further validate the effectiveness of SBDE and the practical application value of its edited defect images in bolt defect detection tasks, we propose the ERA strategy to augment the BDD dataset and evaluate defect detection performance on state-of-the-art detection models. Specifically, we screened normal bolt instances with a resolution greater than 64×64 from BDD as the editing objects. These instances were transformed into defective bolts using SBDE, and their

TABLE VI
RESULTS OF COMPARATIVE EXPERIMENT ON BOLT-SAM SEGMENTATION. THE BEST RESULTS ARE MARKED IN BOLD.

Method	Pin			Nut		
	mIoU(%) ↑	Dice(%) ↑	PA(%) ↑	mIoU(%) ↑	Dice(%) ↑	PA(%) ↑
SAM 1-point [21]	72.06	82.82	97.21	75.17	85.29	94.09
SAM 3-points [21]	71.42	82.35	97.00	75.34	85.40	94.12
SAM-Adapter 1-point [25]	62.37	75.75	96.93	41.56	53.49	87.47
SAM-Adapter 3-points [25]	67.79	80.08	97.20	51.30	63.86	88.59
HQ-SAM 1-point [24]	60.40	74.51	96.60	57.02	70.85	87.04
HQ-SAM 3-points [24]	65.28	78.33	96.68	59.10	72.71	87.05
RobustSAM 1-point [26]	69.15	81.35	97.38	69.51	81.25	92.64
RobustSAM 3-points [26]	71.16	82.80	97.48	70.44	81.90	92.76
Bolt-SAM 1-point	72.73	82.88	97.61	75.24	85.31	94.25
Bolt-SAM 3-points	75.66	86.01	98.02	76.78	86.47	94.71

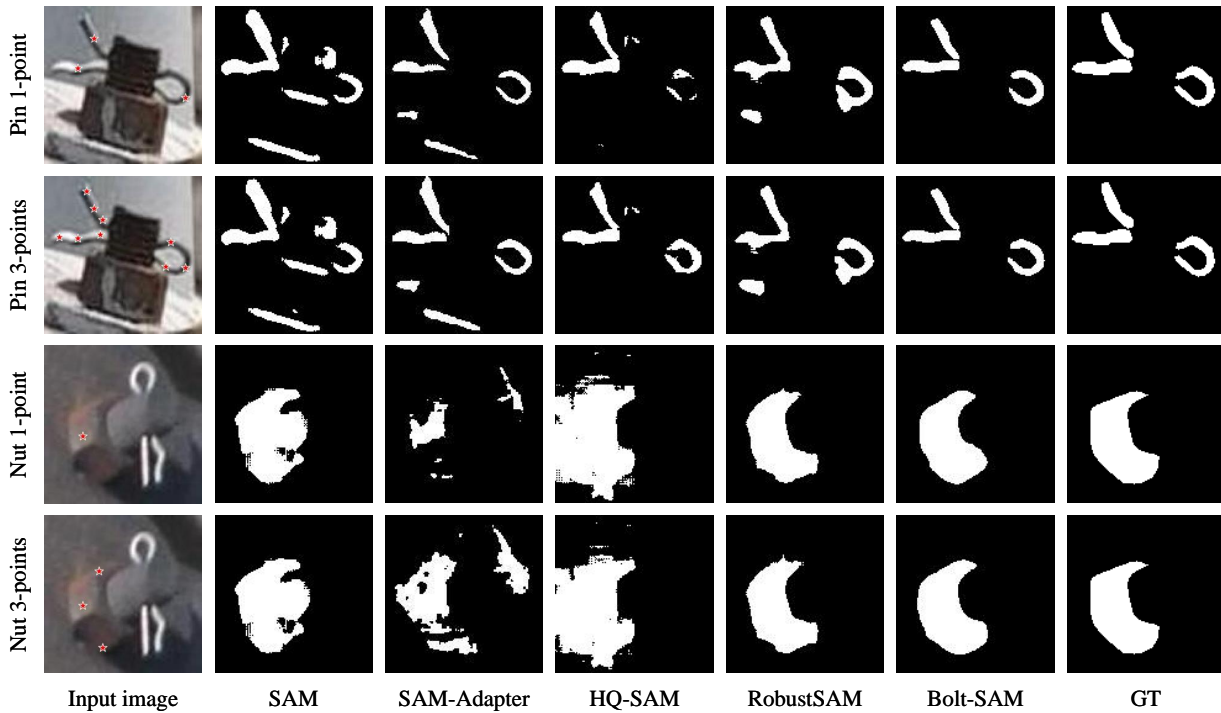


Fig. 8. Visualization of Comparative Experiment for Bolt-SAM Segmentation

TABLE VII
RESULTS OF COMPARATIVE EXPERIMENT ON SBDE EDITING. THE BEST RESULTS ARE MARKED IN BOLD.

Method	Generator	Pin			Nut		
		SSIM(%) ↑	PSNR ↑	LPIPS(%) ↓	SSIM(%) ↑	PSNR ↑	LPIPS(%) ↓
StarGAN-v2 [31]	-	40.52	11.58	89.22	32.97	11.04	78.44
ReStyle+e4e [18], [19]	StyleGAN2-ada [33]	53.64	16.10	62.51	49.63	15.92	56.76
Null-text Inversion [40]	Stable Diffusion [36] +DreamBooth [38]	81.46	17.72	46.03	79.01	19.07	36.64
Negative Inversion [41]		80.31	17.39	48.24	78.85	18.19	39.23
PnP Inversion [42]		79.13	17.19	50.55	78.23	18.12	40.07
SBDE(ours)	-	88.94	23.54	19.05	83.39	21.95	14.97

corresponding labels were modified to create new inspection images with defects, as illustrated in Fig. 1.

Currently, there are no methods directly designed to edit bolt targets within inspection images. Existing bolt editing and generation methods, when combined with the ERA strategy to recover edited bolts to the original image, often result

in artifacts and unnatural discontinuities around the target area, leading to suboptimal performance. Therefore, we chose a copy-based approach as the control group [50]. The data distribution after augmentation is shown in Table VIII. In the experiments, only the training set was augmented, while the test set remained unchanged. Notably, copied images are

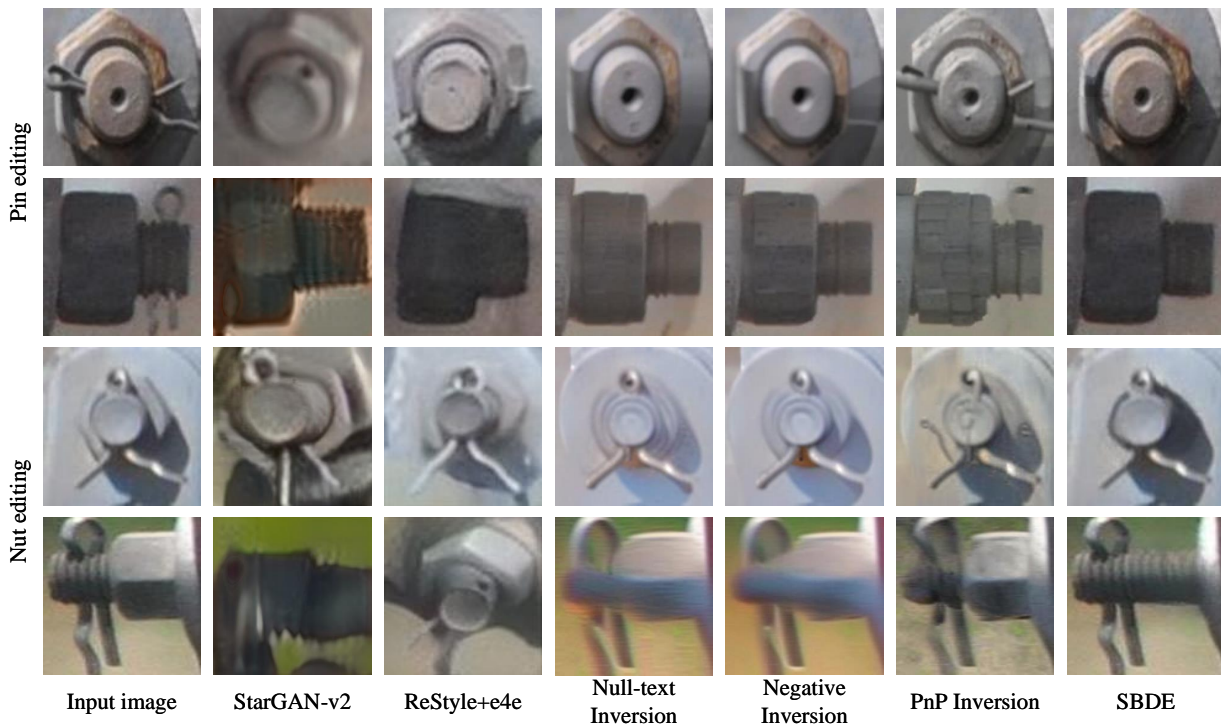


Fig. 9. Visualization of Comparative Experiment for SBDE Editing

TABLE VIII
DATA DISTRIBUTION OF THE TRAINING SET AFTER AUGMENTATION WITH DIFFERENT METHODS.

Class	Original	Copy-aug	SBDE-aug
Inspection images	1433	+759	+759
Number of instances			
Normal	3961	+2872	+1393
Pin losing	449	+192	+1179
Nut losing	244	+36	+528
All	4654	+3100	+3100

TABLE IX
COMPARISON OF DETECTION RESULTS OF DIFFERENT AUGMENTATIONS. THE BEST RESULTS ON THE ENTIRE DATASET ARE MARKED IN BOLD.

Method	Class	P(%)	R(%)	mAP ₅₀ (%)	mAP _{50:95} (%)
Original	All	86.0	76.0	83.1	46.8
	Normal	85.5	86.0	91.0	51.2
	Pin losing	76.4	70.9	77.8	39.9
	Nut losing	96.0	71.1	80.6	49.4
Copy-aug	All	84.2	77.8	84.5	46.2
	Normal	81.2	89.7	90.6	51.8
	Pin losing	74.8	70.3	79.0	40.7
	Nut losing	96.5	73.3	83.9	46.2
SBDE-aug	All	88.2	78.3	87.5	47.8
	Normal	83.1	88.7	91.2	52.4
	Pin losing	82.0	71.0	81.9	42.1
	Nut losing	99.4	75.2	89.3	48.9

identical to the original pre-edited images. We used YOLOv11 as the detection model and evaluated performance using P, R, and mAP. All experiments were conducted under the same hyperparameter settings. The quantitative results in Table IX demonstrate that the SBDE-augmented dataset significantly improved bolt defect detection performance. Compared to the original dataset, SBDE-Aug achieved improvements of 2.2, 2.3, 4.4, and 1.0 in P, R, mAP₅₀, and mAP_{50:95}, respectively, effectively enhancing the model’s ability to detect defective bolts. SBDE-Aug also outperformed Copy-Aug across all metrics, showing a clear advantage. The visual results of bolt defect detection are shown in Fig. 10. SBDE-Aug achieved the best detection performance, while the original detection model and Copy-Aug both exhibited instances of missed detections. Our method provides an effective solution for defect detection with limited defect data and has potential value in practical industrial applications.

V. CONCLUSION

To address the scarcity of bolt defect samples and the imbalance in data distribution in transmission lines, this paper proposes a segmentation-driven bolt defect editing method, named SBDE. The goal is to convert normal bolts into defective ones to augment datasets and improve defect detection performance. We proposed the Bolt-SAM and designed the CFA and MAMD modules to enhance the segmentation accuracy of complex bolt structures. In the editing phase, we designed the MOD module to optimize the attribute segmentation masks and achieved precise attribute editing using MOD-LaMa, generating corresponding defect samples. Additionally, we proposed the ERA strategy to recover the edited defect bolts into the original inspection images, thereby expanding the defect detection dataset and improving the accuracy of bolt

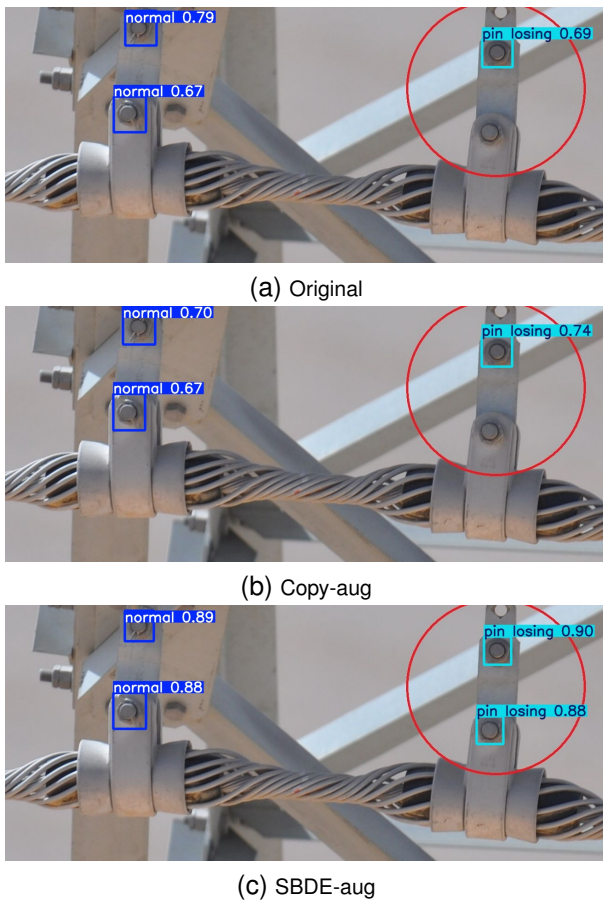


Fig. 10. Visualization of Detection Results with Different Augmentation Methods. The dark blue boxes represent normal bolts, while the light blue boxes indicate bolts losing pins. It is important to note that the red circles are part of the original dataset we collected, not processed by us.

defect detection. Our proposed method offers an innovative solution to the problem of sample scarcity in transmission lines and demonstrates potential applicability in other domains.

Although the proposed SBDE method has achieved good results in bolt editing, its performance is still affected by the pixel quality of the original images. In the future, we plan to integrate it with generative models, leveraging their powerful generation capabilities in general domains to further enhance the quality of defect editing.

REFERENCES

- [1] P. Luo, B. Wang, H. Wang, F. Ma, H. Ma, and L. Wang, "An ultrasmall bolt defect detection method for transmission line inspection," *IEEE Transactions on Instrumentation and Measurement*, vol. 72, pp. 1–12, 2023.
- [2] X. Tao, D. Zhang, Z. Wang, X. Liu, H. Zhang, and D. Xu, "Detection of power line insulator defects using aerial images analyzed with convolutional neural networks," *IEEE Transactions on Systems, Man, and Cybernetics: Systems*, vol. 50, no. 4, pp. 1486–1498, 2020.
- [3] W. Li, H. Wei, Y. Wu, J. Yang, Y. Ruan, Y. Li, and Y. Tang, "Tide: Test-time few-shot object detection," *IEEE Transactions on Systems, Man, and Cybernetics: Systems*, vol. 54, no. 11, pp. 6500–6509, 2024.
- [4] K. Zhang, R. Zhou, J. Wang, Y. Xiao, X. Guo, and C. Shi, "Transmission line component defect detection based on uav patrol images: A self-supervised hc-vit method," *IEEE Transactions on Systems, Man, and Cybernetics: Systems*, vol. 54, no. 11, pp. 6510–6521, 2024.

- [5] Y. Chen, Z.-W. Liu, G. Wen, and Y.-W. Wang, "Distributed finite-time observer for multiple line outages detection in power systems," *IEEE Transactions on Systems, Man, and Cybernetics: Systems*, vol. 54, no. 3, pp. 1768–1778, 2024.
- [6] K. Zhang, Y. Xiao, J. Wang, M. Du, X. Guo, R. Zhou, C. Shi, and Z. Zhao, "Dp-gan: A transmission line bolt defects generation network based on dual discriminator architecture and pseudo-enhancement strategy," *IEEE Transactions on Power Delivery*, vol. 39, no. 3, pp. 1622–1633, 2024.
- [7] Y. Ren, J. Liu, H. Zhao, and H. Zhang, "An industrial fault sample reconstruction and generation method under limited samples with missing information," *IEEE Transactions on Systems, Man, and Cybernetics: Systems*, vol. 54, no. 12, pp. 7821–7833, 2024.
- [8] S. Niu, B. Li, X. Wang, and H. Lin, "Defect image sample generation with gan for improving defect recognition," *IEEE Transactions on Automation Science and Engineering*, vol. 17, no. 3, pp. 1611–1622, 2020.
- [9] Y. Duan, Y. Hong, L. Niu, and L. Zhang, "Few-shot defect image generation via defect-aware feature manipulation," in *Proceedings of the AAAI Conference on Artificial Intelligence*, vol. 37, no. 1, 2023, pp. 571–578.
- [10] T. Karras, S. Laine, M. Aittala, J. Hellsten, J. Lehtinen, and T. Aila, "Analyzing and improving the image quality of stylegan," in *Proceedings of the IEEE/CVF conference on computer vision and pattern recognition*, 2020, pp. 8110–8119.
- [11] G. Zhang, K. Cui, T.-Y. Hung, and S. Lu, "Defect-gan: High-fidelity defect synthesis for automated defect inspection," in *Proceedings of the IEEE/CVF Winter Conference on Applications of Computer Vision*, 2021, pp. 2524–2534.
- [12] F. Deng, J. Luo, L. Fu, Y. Huang, J. Chen, N. Li, J. Zhong, and T. L. Lam, "Dg2gan: improving defect recognition performance with generated defect image sample," *Scientific Reports*, vol. 14, no. 1, p. 14787, 2024.
- [13] Y. Tai, K. Yang, T. Peng, Z. Huang, and Z. Zhang, "Defect image sample generation with diffusion prior for steel surface defect recognition," *arXiv preprint arXiv:2405.01872*, 2024.
- [14] E. Härkönen, A. Hertzmann, J. Lehtinen, and S. Paris, "Ganspace: Discovering interpretable gan controls," *Advances in neural information processing systems*, vol. 33, pp. 9841–9850, 2020.
- [15] Y. Shen and B. Zhou, "Closed-form factorization of latent semantics in gans," in *Proceedings of the IEEE/CVF conference on computer vision and pattern recognition*, 2021, pp. 1532–1540.
- [16] B. Wallace, A. Gokul, and N. Naik, "Edict: Exact diffusion inversion via coupled transformations," in *Proceedings of the IEEE/CVF Conference on Computer Vision and Pattern Recognition*, 2023, pp. 22532–22541.
- [17] E. Richardson, Y. Alaluf, O. Patashnik, Y. Nitzan, Y. Azar, S. Shapiro, and D. Cohen-Or, "Encoding in style: a stylegan encoder for image-to-image translation," in *Proceedings of the IEEE/CVF conference on computer vision and pattern recognition*, 2021, pp. 2287–2296.
- [18] O. Tov, Y. Alaluf, Y. Nitzan, O. Patashnik, and D. Cohen-Or, "Designing an encoder for stylegan image manipulation," *ACM Transactions on Graphics (TOG)*, vol. 40, no. 4, pp. 1–14, 2021.
- [19] Y. Alaluf, O. Patashnik, and D. Cohen-Or, "Restyle: A residual-based stylegan encoder via iterative refinement," in *Proceedings of the IEEE/CVF international conference on computer vision*, 2021, pp. 6711–6720.
- [20] Z. Zhao, H. Qi, Y. Qi, K. Zhang, Y. Zhai, and W. Zhao, "Detection method based on automatic visual shape clustering for pin-missing defect in transmission lines," *IEEE Transactions on Instrumentation and Measurement*, vol. 69, no. 9, pp. 6080–6091, 2020.
- [21] A. Kirillov, E. Mintun, N. Ravi, H. Mao, C. Rolland, L. Gustafson, T. Xiao, S. Whitehead, A. C. Berg, W.-Y. Lo *et al.*, "Segment anything," in *Proceedings of the IEEE/CVF International Conference on Computer Vision*, 2023, pp. 4015–4026.
- [22] Y. Gu, Q. Wu, H. Tang, X. Mai, H. Shu, B. Li, and Y. Chen, "Lesam: Adapt segment anything model for medical lesion segmentation," *IEEE Journal of Biomedical and Health Informatics*, 2024.
- [23] Y. Zhang, Z. Shen, and R. Jiao, "Segment anything model for medical image segmentation: Current applications and future directions," *Computers in Biology and Medicine*, p. 108238, 2024.
- [24] L. Ke, M. Ye, M. Danelljan, Y.-W. Tai, C.-K. Tang, F. Yu *et al.*, "Segment anything in high quality," *Advances in Neural Information Processing Systems*, vol. 36, 2024.
- [25] T. Chen, L. Zhu, C. Deng, R. Cao, Y. Wang, S. Zhang, Z. Li, L. Sun, Y. Zang, and P. Mao, "Sam-adapter: Adapting segment anything in underperformed scenes," in *Proceedings of the IEEE/CVF International Conference on Computer Vision*, 2023, pp. 3367–3375.

- [26] W.-T. Chen, Y.-J. Vong, S.-Y. Kuo, S. Ma, and J. Wang, "Robustsam: Segment anything robustly on degraded images," in *Proceedings of the IEEE/CVF Conference on Computer Vision and Pattern Recognition*, 2024, pp. 4081–4091.
- [27] H. Dai, C. Ma, Z. Yan, Z. Liu, E. Shi, Y. Li, P. Shu, X. Wei, L. Zhao, Z. Wu *et al.*, "Samaug: Point prompt augmentation for segment anything model," *arXiv preprint arXiv:2307.01187*, 2023.
- [28] T. Yu, R. Feng, R. Feng, J. Liu, X. Jin, W. Zeng, and Z. Chen, "Inpaint anything: Segment anything meets image inpainting," *arXiv preprint arXiv:2304.06790*, 2023.
- [29] A. Melnik, M. Miasayedzenkau, D. Makaravets, D. Pirshuk, E. Akbulut, D. Holzmann, T. Rensch, G. Reichert, and H. Ritter, "Face generation and editing with stylegan: A survey," *IEEE Transactions on Pattern Analysis and Machine Intelligence*, 2024.
- [30] Y. Choi, M. Choi, M. Kim, J.-W. Ha, S. Kim, and J. Choo, "Stargan: Unified generative adversarial networks for multi-domain image-to-image translation," in *Proceedings of the IEEE Conference on Computer Vision and Pattern Recognition (CVPR)*, 2018.
- [31] Y. Choi, Y. Uh, J. Yoo, and J.-W. Ha, "Stargan v2: Diverse image synthesis for multiple domains," in *Proceedings of the IEEE/CVF Conference on Computer Vision and Pattern Recognition (CVPR)*, 2020.
- [32] T. Karras, S. Laine, and T. Aila, "A style-based generator architecture for generative adversarial networks," *IEEE Transactions on Pattern Analysis and Machine Intelligence*, vol. 43, no. 12, pp. 4217–4228, 2021.
- [33] T. Karras, M. Aittala, J. Hellsten, S. Laine, J. Lehtinen, and T. Aila, "Training generative adversarial networks with limited data," in *Advances in Neural Information Processing Systems*, 2020.
- [34] J. Ho, A. Jain, and P. Abbeel, "Denoising diffusion probabilistic models," *Advances in neural information processing systems*, vol. 33, pp. 6840–6851, 2020.
- [35] J. Song, C. Meng, and S. Ermon, "Denoising diffusion implicit models," *arXiv preprint arXiv:2010.02502*, 2020.
- [36] R. Rombach, A. Blattmann, D. Lorenz, P. Esser, and B. Ommer, "High-resolution image synthesis with latent diffusion models," in *Proceedings of the IEEE/CVF conference on computer vision and pattern recognition*, 2022, pp. 10 684–10 695.
- [37] R. Gal, Y. Alaluf, Y. Atzmon, O. Patashnik, A. H. Bermano, G. Chechik, and D. Cohen-Or, "An image is worth one word: Personalizing text-to-image generation using textual inversion," *arXiv preprint arXiv:2208.01618*, 2022.
- [38] N. Ruiz, Y. Li, V. Jampani, Y. Pritch, M. Rubinstein, and K. Aberman, "Dreambooth: Fine tuning text-to-image diffusion models for subject-driven generation," in *Proceedings of the IEEE/CVF conference on computer vision and pattern recognition*, 2023, pp. 22 500–22 510.
- [39] E. J. Hu, Y. Shen, P. Wallis, Z. Allen-Zhu, Y. Li, S. Wang, L. Wang, and W. Chen, "Lora: Low-rank adaptation of large language models," *arXiv preprint arXiv:2106.09685*, 2021.
- [40] R. Mokady, A. Hertz, K. Aberman, Y. Pritch, and D. Cohen-Or, "Null-text inversion for editing real images using guided diffusion models," in *Proceedings of the IEEE/CVF Conference on Computer Vision and Pattern Recognition*, 2023, pp. 6038–6047.
- [41] D. Miyake, A. Iohara, Y. Saito, and T. Tanaka, "Negative-prompt inversion: Fast image inversion for editing with text-guided diffusion models," *arXiv preprint arXiv:2305.16807*, 2023.
- [42] X. Ju, A. Zeng, Y. Bian, S. Liu, and Q. Xu, "Direct inversion: Boosting diffusion-based editing with 3 lines of code," *arXiv preprint arXiv:2310.01506*, 2023.
- [43] R. Suvorov, E. Logacheva, A. Mashikhin, A. Remizova, A. Ashukha, A. Silvestrov, N. Kong, H. Goka, K. Park, and V. Lempitsky, "Resolution-robust large mask inpainting with fourier convolutions," in *Proceedings of the IEEE/CVF winter conference on applications of computer vision*, 2022, pp. 2149–2159.
- [44] K. Zhang, W. Lou, J. Wang, R. Zhou, X. Guo, Y. Xiao, C. Shi, and Z. Zhao, "Pa-detr: End-to-end visually indistinguishable bolt defects detection method based on transmission line knowledge reasoning," *IEEE Transactions on Instrumentation and Measurement*, vol. 72, pp. 1–14, 2023.
- [45] N. Carion, F. Massa, G. Synnaeve, N. Usunier, A. Kirillov, and S. Zagoruyko, "End-to-end object detection with transformers," in *European conference on computer vision*. Springer, 2020, pp. 213–229.
- [46] S. M. Pizer, E. P. Amburn, J. D. Austin, R. Cromartie, A. Geselowitz, T. Greer, B. ter Haar Romeny, J. B. Zimmerman, and K. Zuiderveld, "Adaptive histogram equalization and its variations," *Computer vision, graphics, and image processing*, vol. 39, no. 3, pp. 355–368, 1987.
- [47] W. Liu, X. Shen, C.-M. Pun, and X. Cun, "Explicit visual prompting for low-level structure segmentations," in *Proceedings of the IEEE/CVF Conference on Computer Vision and Pattern Recognition*, 2023, pp. 19 434–19 445.
- [48] D. Hendrycks and K. Gimpel, "Gaussian error linear units (gelus)," *arXiv preprint arXiv:1606.08415*, 2016.
- [49] R. Khanam and M. Hussain, "Yolov11: An overview of the key architectural enhancements," *arXiv preprint arXiv:2410.17725*, 2024.
- [50] J. Liu, Z. Ma, Y. Qiu, X. Ni, B. Shi, and H. Liu, "Four discriminator cycle-consistent adversarial network for improving railway defective fastener inspection," *IEEE Transactions on Intelligent Transportation Systems*, vol. 23, no. 8, pp. 10 636–10 645, 2021.